Supporting Information for "The Biosphere Under Potential Paris Outcomes"

Sebastian Ostberg[1,2], Lena R. Boysen[1,3], Sibyll Schaphoff[1], Wolfgang Lucht[1,2], and Dieter Gerten[1,2]

Contents of this file

Introduction

This Supporting Information provides further methodological details regarding the Γ metric (Texts S1 and S2, Tables S1 and S2), land use input data (Text S3, Figures S1 and S2) and the biome classification used in this study to aggregate grid-cell results (Text S4, Figures S3 and S4). Figures S5 and S6 show additional results discussed in the main paper. Text S5 and Figure S7 present a decomposition of the full Γ metric into its components. Text S6, Figures S8 and S9 present a sensitivity analysis.

Text S1 ΔV metric description.

Originally developed by *Sykes et al.* [1999] and extended by *Ostberg et al.* [2015], ΔV measures the difference in vegetation structure in terms of the importance of broad life form types (grass, trees, bare ground), further characterized by a series of life-form specific attributes a.

$$\Delta V(i,j) = 1 - \sum_k \left\{ min(V_{ik}, V_{jk}) * \left[1 - \sum_l (\omega_{kl} * |a_{ikl} - a_{jkl}|) \right] \right\} \tag{1}$$

V_{ik} and V_{jk} represent the area fractions covered by life form k in landscapes i and j, a_{ikl} and a_{jkl} represent attribute l of life form k in i and j, respectively. Attributes are weighted for each life form by ω_{kl}. Plant-functional types (PFTs), crop-functional types (CFTs) and biomass-functional types (BFTs) from LPJmL are each grouped by life form k and assigned attributes according to Table S2. Attributes evergreenness, needleleavedness, tropicalness and borealness are taken over from the original implementation by *Sykes et al.* [1999], while naturalness was added by *Ostberg et al.* [2015] to distinguish crops (and now also bioenergy plantations) from natural vegetation.

Text S2 Vector geometry and scaling of Γ metric

The calculation of the Γ metric follows *Heyder et al.* [2011]. Two ecosystem states are expressed by state vec-

---

[1]Earth System Analysis, Potsdam Institute for Climate Impact Research (PIK), Member of the Leibniz Association, Potsdam, Germany

[2]Geography Department, Humboldt-Universität zu Berlin, Berlin, Germany

[3]Land in the Earth System, Max Planck Institute for Meteorology, Hamburg, Germany

tors $\vec{s_1}$ and $\vec{s_2}$ for variables $v_i, i = [1, \ldots, n]$:

$$\vec{s_1} = \begin{pmatrix} v_{1,1} \\ \vdots \\ v_{n,1} \end{pmatrix}, \vec{s_2} = \begin{pmatrix} v_{1,2} \\ \vdots \\ v_{n,2} \end{pmatrix}, \tag{2}$$

where $\vec{s_1}$ represents the reference state and $\vec{s_2}$ the changed state under climate change and/or land use change, with v_i given by the parameters in Table S1 except those for vegetation structure. Since the values of state parameters v_i can differ by several orders of magnitude they are normalized. For local change c state parameters are normalized to the local value of v_i under reference conditions, leading to:

$$\vec{s_{l_1}} = \begin{pmatrix} 1 \\ \vdots \\ 1 \end{pmatrix}, \vec{s_{l_2}} = \begin{pmatrix} v_{1,l} \\ \vdots \\ v_{n,l} \end{pmatrix} \tag{3}$$

where

$$v_{i,l} = \frac{v_{i,2}}{v_{i,1}}, \quad \text{for } v_{i,1} \neq 0. \tag{4}$$

For global importance g state vectors are normalized to the global, spatially averaged mean value of v_i under reference conditions, resulting in:

$$\vec{s_{g_1}} = \begin{pmatrix} v_{1,g,1} \\ \vdots \\ v_{n,g,1} \end{pmatrix}, \vec{s_{g_2}} = \begin{pmatrix} v_{1,g,2} \\ \vdots \\ v_{n,g,2} \end{pmatrix} \tag{5}$$

where

$$v_{i,g,t} = \frac{v_{i,t}}{\overline{v_{i,\text{refg}}}}, \quad \text{for } \overline{v_{i,\text{refg}}} \neq 0 \tag{6}$$

and

$$\overline{v_{i,\text{refg}}} = \frac{1}{\sum a_p} \sum_{p=1}^z a_p v_{i,p} \tag{7}$$

for cells $p = 1, \ldots, z$ with cell area a_p.

The difference d between two states is calculated as the magnitude of the difference vector $\vec{d}$. For local change c

$$d_c = |\vec{d_c}| = |\vec{s_{l_2}} - \vec{s_{l_1}}| \tag{8}$$

while for global importance g

$$d_g = |\vec{d_g}| = |\vec{s_{g_2}} - \vec{s_{g_1}}|. \tag{9}$$

Shifts in the balance b' of ecosystem processes are calculated as the angle α between two state vectors with local normalization:

$$b' = 1 - \cos\alpha = 1 - \frac{\vec{s_{l_1}} \cdot \vec{s_{l_2}}}{|\vec{s_{l_1}}||\vec{s_{l_2}}|}. \tag{10}$$

If the relative contributions of all parameters v_i are constant the direction of $\vec{s_{l_1}}$ and $\vec{s_{l_2}}$ is identical and $\cos\alpha = 1$. For orthogonal state vectors $\cos\alpha = 0$, whereas $\cos\alpha = -1$ if both state vectors are opposed. b' is scaled to a range between 0 and 1 assigning a value of 1 if the angle between

state vectors is larger than 60°:

$$b = \begin{cases} b' \cdot 2 & \text{for } \alpha \leq 60° \\ 1 & \text{for } \alpha > 60° \end{cases} \quad (11)$$

Values for metric components c and g are derived by scaling d_c and d_g to a range between 0 and 1 using the following sigmoid transformation function T:

$$c = T(d_c), \quad g = T(d_g), \quad (12)$$

with

$$T(x) = A + \frac{1 - A}{1 + e^{-6(x-0.5)}} \quad (13)$$

where $A = -\frac{1}{e^3}$. The transformation function assigns a value of 0 in case of 'no change' and $T(x) \geq 0.95$ if the change is larger than one mean value.
The change-to-variability ratio $S(x, \sigma_x)$ for components $x(d_c, d_g, b'$ and $\Delta V)$ is calculated as

$$S(x, \sigma_x) = \frac{1}{1 + e^{-4(\frac{x}{\sigma_x} - 2)}} \quad (14)$$

with σ_x the interannual standard deviation of x under reference conditions. This transformation function assigns values of $S \leq 0.018$ to changes within one standard deviation, $S = 0.5$ to changes of two standard deviations and $S \geq 0.982$ to changes larger than three standard deviations. For full details see *Heyder et al.* [2011]. Text S5 and Figure S7 illustrate the contribution of the different components to the full metric value in major biomes.

Text S3 Filtering of unproductive bioenergy tree plantations.

Figure S1 shows the fraction of each grid cell covered by 3 major land use types (cropland, pasture, bioenergy plantations) for the end of the historical period (1976–2005) as well as the end of all four scenarios (2070–2099). Bioenergy fractions under RCP2.6 and RCP6.0 are assumed to be covered with 50% bioenergy grass and 50% bioenergy tree plantations. However, climate conditions in some of the grid cells with bioenergy fractions do not support tree growth, causing planted bioenergy trees to die. If this happens repeatedly dead biomass will accumulate in the modeled litter and soil carbon pools. Since carbon contained in the sapling is subtracted from harvest it can also lead to negative harvest values. To avoid this, all LUC$_{noCC}$ and LUC$_{CC}$ simulations for RCP2.6 and RCP6.0 are run twice. After the first run, all grid cells where either mean harvest averaged over all climate models is below $100 \, \text{g/m}^2$ of carbon or harvest is negative in at least one simulation are marked as unproductive. This means that the bioenergy tree fraction in the land use input is reassigned to bioenergy grass in all years following the first unproductive harvest. In case a grid cell returns to productive conditions at a later year of the test simulations, bioenergy tree plantations can be restored. The updated land use patterns are then applied to all climate models during the second iteration of LUC$_{noCC}$ and LUC$_{CC}$ simulations. Results from this second iteration are used in the calculation of the Γ metric. Figure S2 shows bioenergy tree and bioenergy grass areas after filtering. Up to 23% and 13% of global bioenergy tree area is reassigned to bioenergy grass under RCP2.6 and RCP6.0, respectively.

Text S4 Biome classification.

The biome classification follows *Ostberg et al.* [2015]. It is based on the composition of PFTs modeled in LPJmL. An additional tree leaf area index (LAI) limit is used to distinguish between tropical forests and warm woody savannas.

A temperature limit is used to classify tundra. The classification scheme is illustrated in Figure S1 of *Ostberg et al.* [2015]. Figure S3 below shows modeled biome distributions for the end of the historical period (1976–2005) as well as the end of all four scenarios (2070–2099). In cases where LPJmL simulations driven by different climate models do not agree on the biome class in a grid cell the dominant (most frequent) value is shown. Figures S4–S6 as well as Figure 3 in the main text use an aggregated version of this biome classification which distinguishes only one forest type per climate region and combines "woody savanna & woodland", "savanna" and "grassland" biomes into "non-forest".
Figure S4 aggregates the three land use categories from Figure S1 per major biome class and presents the temporal evolution during the 20th and 21st century. While Figure 3 in the main text shows the fraction of biomes projected to experience major full impacts (the combination of climate change and land use change), Figures S5 & S6 present results for the individual effects of climate change and land use change.

Text S5 Metric components

Figure S7 presents a decomposition of the full Γ metric into its components for major biomes and for the climate change effect, land use change effect and full impact. Values for all grid cells belonging to each major biome (see Text S4) are spatially averaged using a cell-area based weighting. Whiskers denote the range across simulations driven by 20 different climate models. Ecosystem balance $b \cdot S(b, \sigma_b)$, global importance $g \cdot S(g, \sigma_g)$, local change $c \cdot S(c, \sigma_c)$ and vegetation structure $\Delta V \cdot S(\Delta V, \sigma_{\Delta V})$ are combined into the full Γ metric (see Equation 1 in the main text). We also provide the combination of ecosystem balance, local change and global importance for the subsets of parameters from Table S1 "carbon exchange fluxes", "carbon stocks" and "water exchange fluxes". On average, changes in tropical forests have the highest global importance g of all biomes across all four scenarios. This means that changes in tropical forests contribute more to global biogeochemical cycles in absolute terms than changes in the other biomes. In contrast, changes in deserts have a low global importance even though local change c and ecosystem balance b may adopt high values. This is because ecosystem state parameters generally have very low values in deserts. Small changes in weather can lead to large relative changes in these parameters — which are captured by b and c — but changes are small in absolute terms (g). Changes to vegetation structure (ΔV) are also generally small in deserts. In tropical and temperate biomes land use usually has a higher impact on vegetation structure (ΔV) than climate change. This is especially true for tropical and temperate forests. Climate-driven changes in vegetation structure are more common in tropical and temperate savanna ecosystems which are often in the transition zone between forests and grasslands. Both boreal forests and tundra regions have low land use change impacts but high climate-driven ΔV values because of woody encroachment into the tundra and drought and heat-related tree mortality along the warm edge of the boreal zone. The metric values for carbon exchange fluxes are often larger than the values for carbon stocks. This is because carbon stocks change only if the balance between inputs and outputs is shifted, not if the relative contribution of fluxes into and out of the biosphere stays constant. Land use change (deforestation) has a strong impact on carbon stocks in forests which is larger than carbon stock changes driven by changes in carbon fluxes. In most biomes changes in water fluxes are smaller than changes in carbon fluxes,

although this difference between carbon flux changes and water flux changes is usually more pronounced for the climate change effect than the land use change effect.

Text S6 Alternative measures of human interference with the biosphere.

A threshold of $\Gamma > 0.3$ is used for the main analysis to distinguish landscapes with major impacts of human interference with the biosphere. Figure S8 presents global results using the globally area-weighted mean value of Γ instead of a threshold. While absolute values are not comparable, the relative ranking of scenarios and the relative strength of climate change effects compared to land use change effects stays the same as in the main results: (1) average CC impacts increase with increasing CC forcing from lowest in the *Paris success* case to highest in the *Paris failure* scenario; (2) average land use change effects are lowest in the *INDC+* and highest in the *Paris success* scenario; (3) average impacts of CC far surpass average LUC impacts by the end of the 21st century in all scenarios except *Paris success*; (4) the average full impact is slightly lower under *INDC+* than *Paris success*. Figure S9 explores different thresholds of the Γ metric. For a very low threshold of $\Gamma > 0.1$, CC impacts may surpass LUC impacts in terms of the affected global area even in the *Paris success* scenario — which means that CC will expose more landscapes globally to at least moderate change than LUC under all four scenarios according to our simulations. On the other hand, the global land area projected to experience at least moderate full impacts — from the combination of CC and LUC — is lowest in the *Paris success* scenario instead of the *INDC+* scenario found in the main results. If higher thresholds than $\Gamma > 0.3$ are used to mark landscapes with major human interference with the biosphere the full impact in the *Paris success* scenario comes progressively closer to the full impact in the *INDC* scenario, suggesting that *INDC+* is more successful than *Paris success* in avoiding increasingly strong human impacts on the biosphere.

References

Heyder, U., S. Schaphoff, D. Gerten, and W. Lucht (2011), Risk of severe climate change impact on the terrestrial biosphere, *Environmental Research Letters*, *6*(3), 034,036, doi: 10.1088/1748-9326/6/3/034036.

Ostberg, S., S. Schaphoff, W. Lucht, and D. Gerten (2015), Three centuries of dual pressure from land use and climate change on the biosphere, *Environmental Research Letters*, *10*, 044011, doi:10.1088/1748-9326/10/4/044011.

Sykes, M. T., I. C. Prentice, and F. Laarif (1999), Quantifying the impact of global climate change on potential natural vegetation, *Climatic change*, *41*, 37–52, doi: 10.1023/A:1005435831549.

Corresponding author: Sebastian Ostberg, Earth System Analysis, Potsdam Institute for Climate Impact Research (PIK), Member of the Leibniz Association, P.O. Box 60 12 03, D-14412, Germany. (ostberg@pik-potsdam.de)
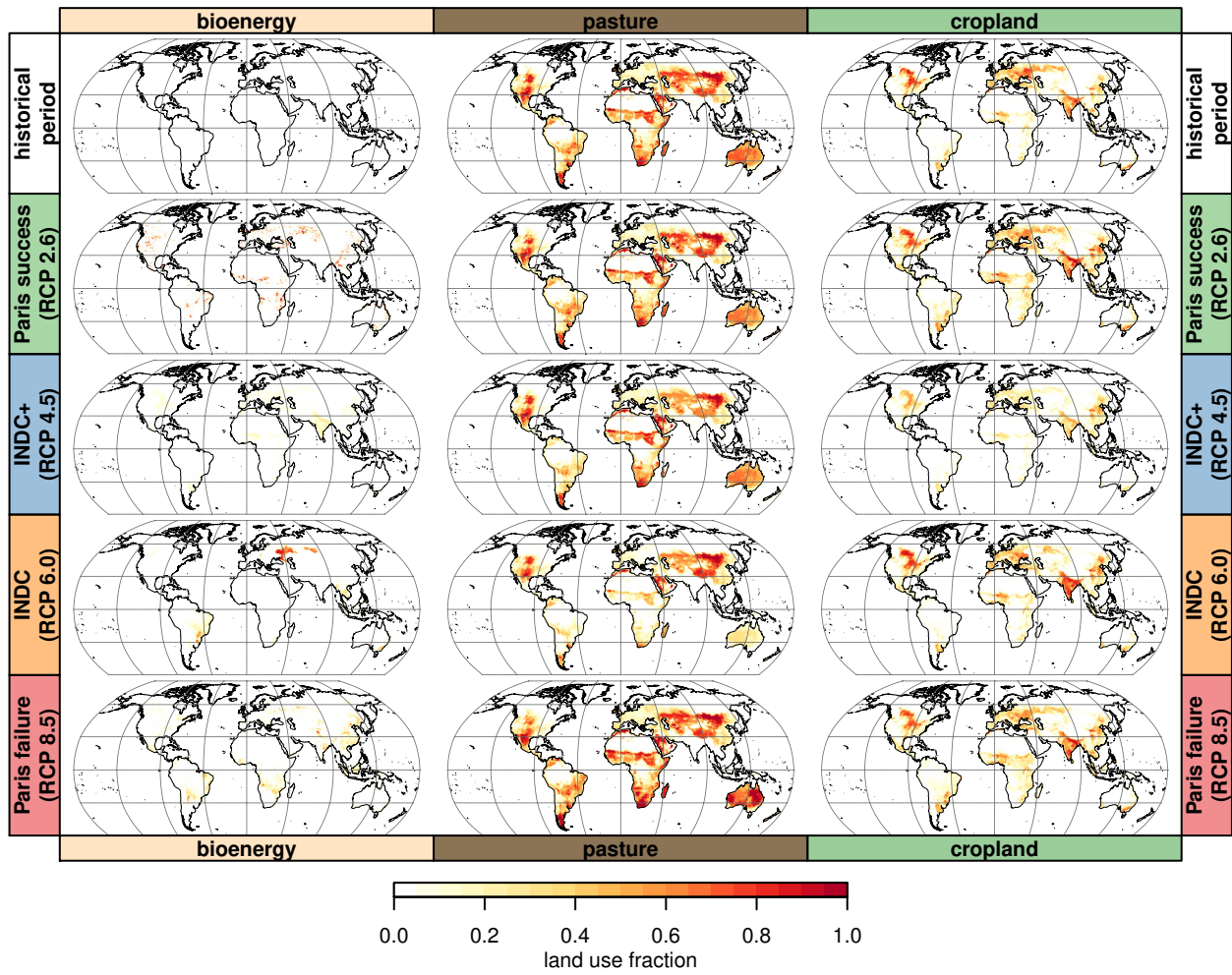
Figure S1. Fraction of each grid cell covered by major types of land use at the end of the historical period (1976–2005) and the end of the four studied scenarios (2070–2099).
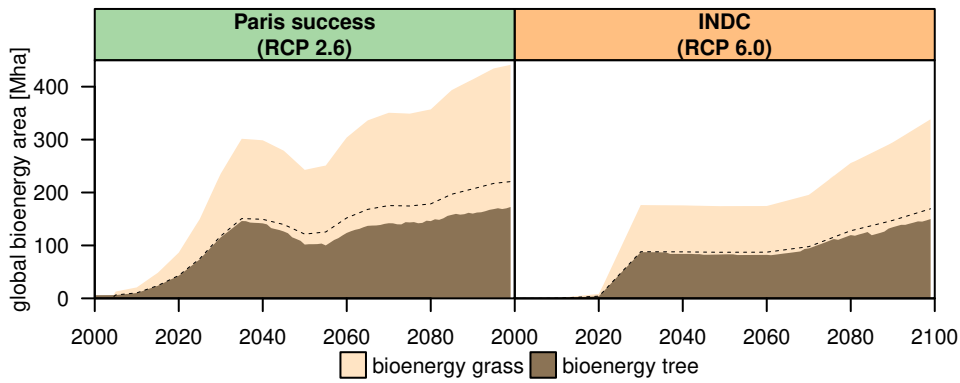

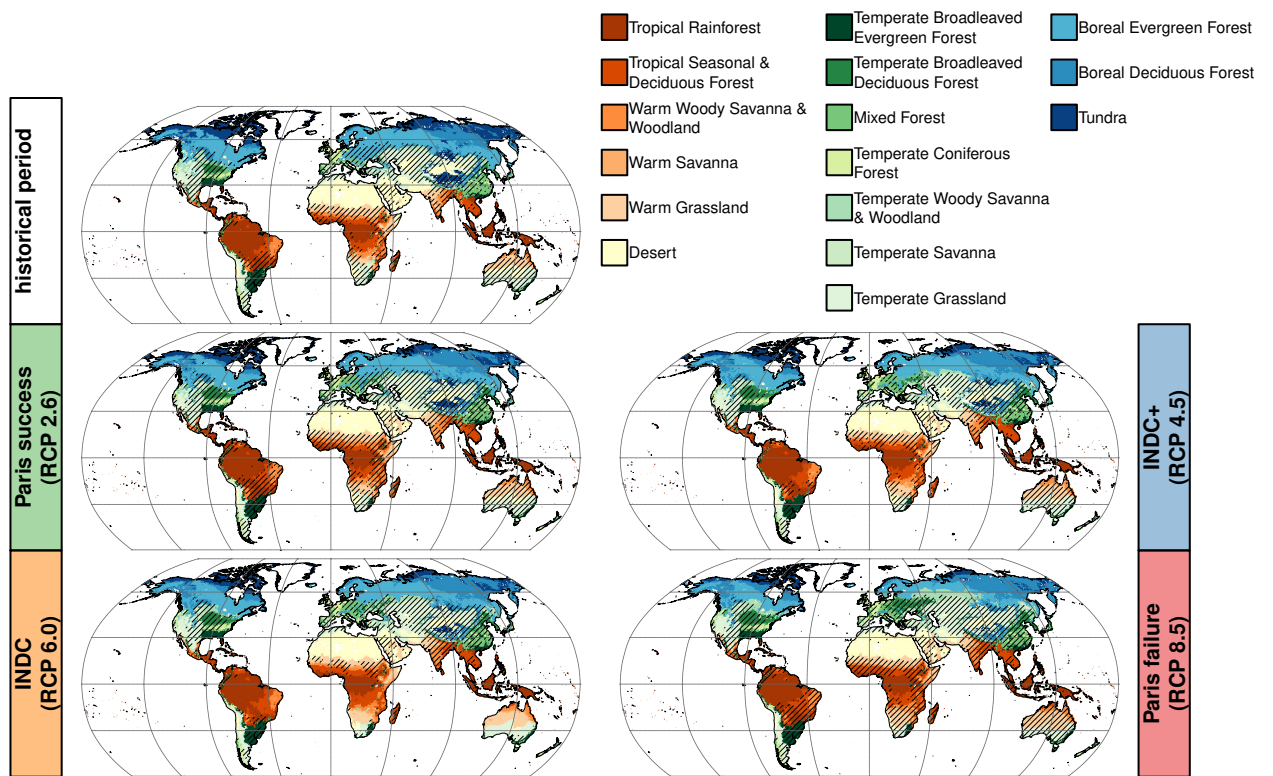**Figure S2.** Bioenergy areas by plantation type after filtering. Dashed line marks 50% share.

Figure S3. Modeled biome distribution. Historical period refers to 1976–2005, all scenarios refer to 2070–2099. Hatching marks grid cells with at least 50% land use.
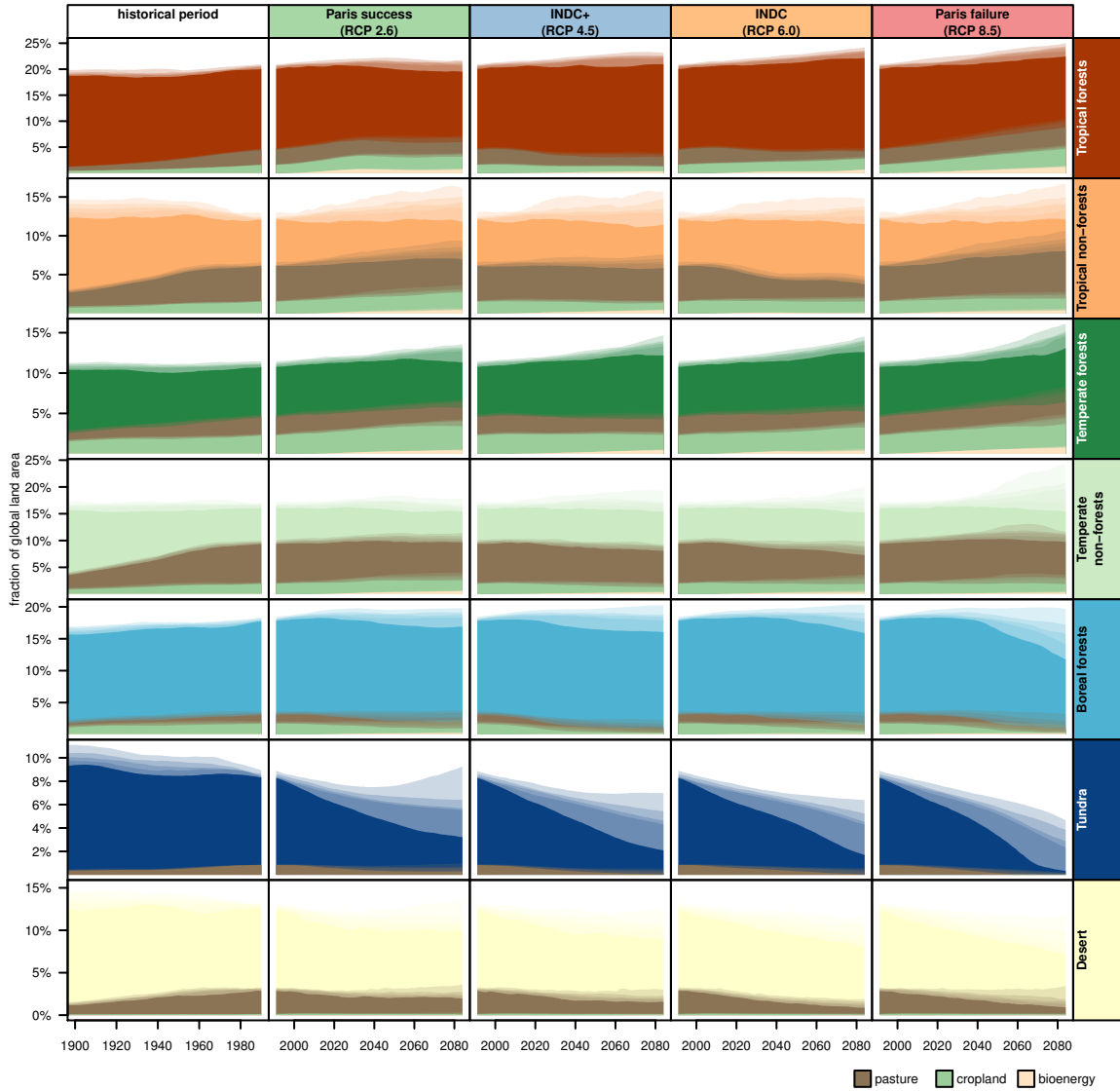
Figure S4. Land use in major biomes over time. Each plot shows the fraction of the global land area covered by the respective biome as well as the fraction of the biome covered by the major types of land use shown in Figure S1. Biome classification of landscapes (grid cells) is based on their potential natural vegetation even if land has been converted to agriculture. As in Figure 3 in the main text, semitransparent shading denotes the uncertainty arising out of using 20 climate models to drive vegetation simulations (maximum, 75%, 50% and 25% quantile and minimum extent).
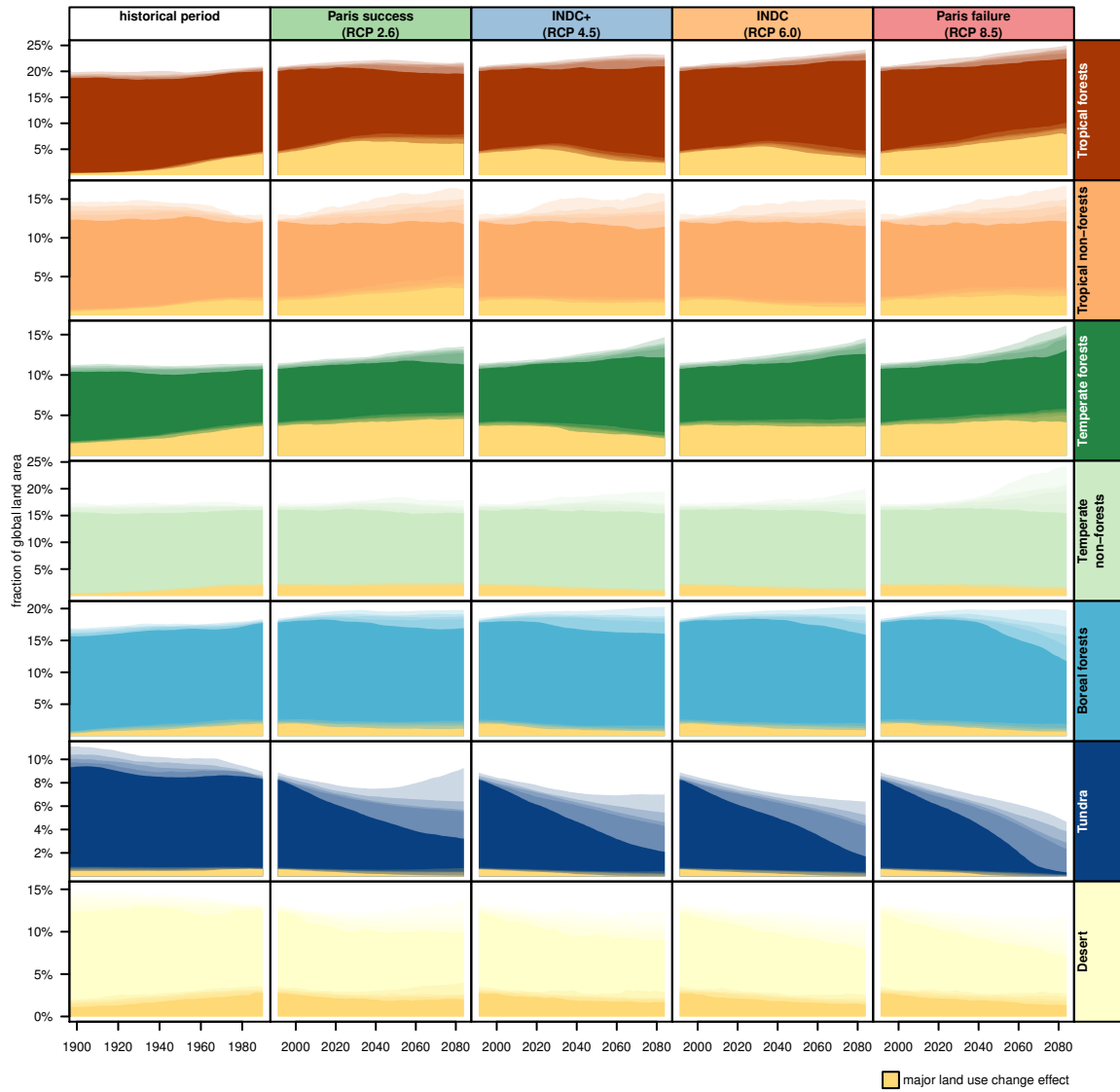
Figure S5. Impacts of land use change in major biomes over time. Each plot shows the fraction of the global land area covered by the respective biome as well as the fraction of the biome projected to experience major change (yellow overlay). As in Figure 3 in the main text, semitransparent shading denotes the uncertainty arising out of using 20 climate models to drive vegetation simulations (maximum, 75%, 50% and 25% quantile and minimum extent).
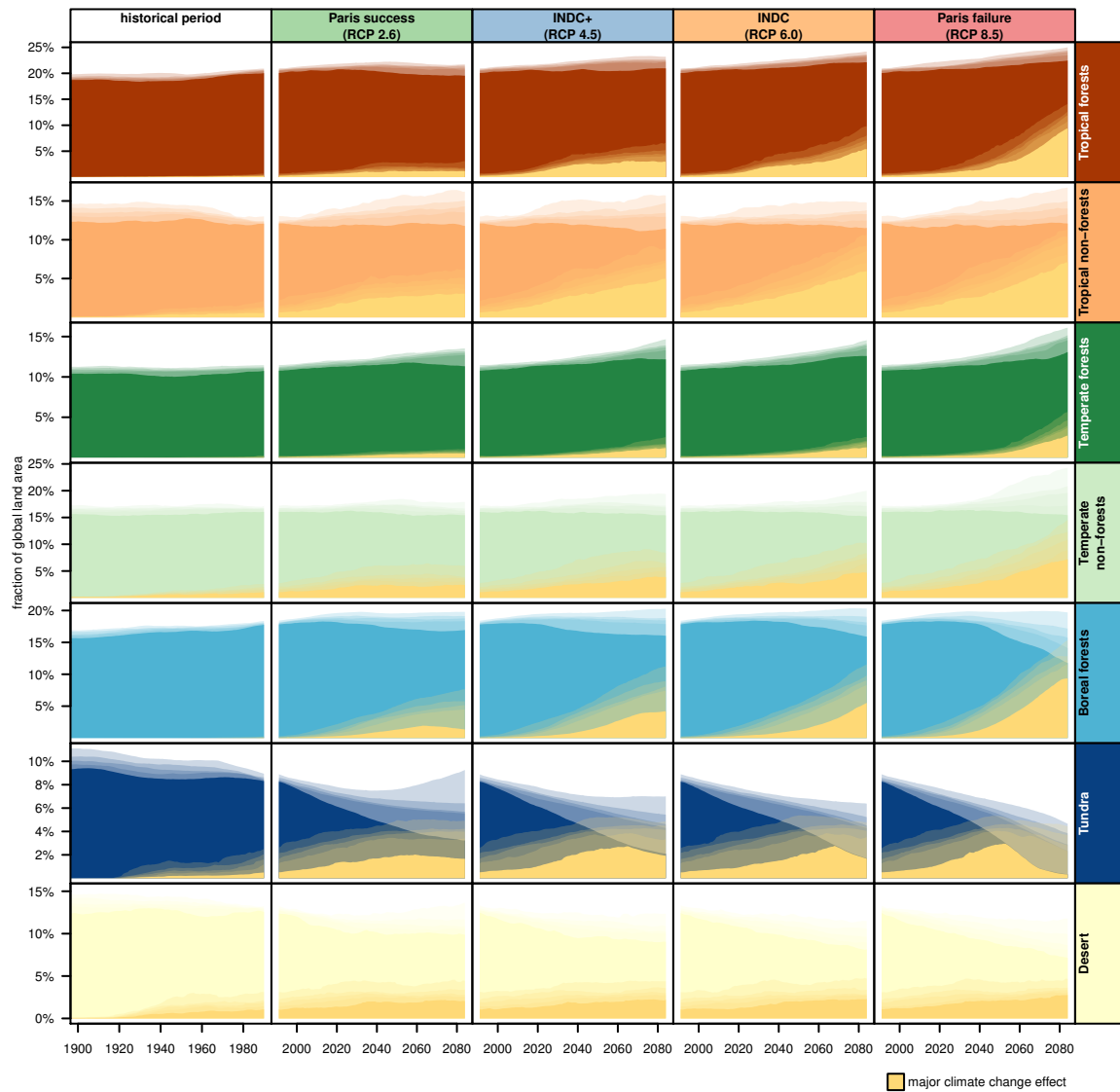
Figure S6. Impacts of climate change in major biomes over time. Each plot shows the fraction of the global land area covered by the respective biome as well as the fraction of the biome projected to experience major change (yellow overlay). As in Figure 3 in the main text, semitransparent shading denotes the uncertainty arising out of using 20 climate models to drive vegetation simulations (maximum, 75%, 50% and 25% quantile and minimum extent).
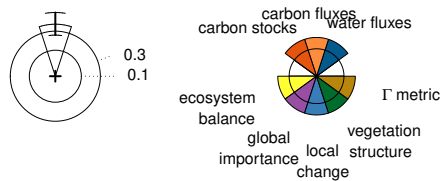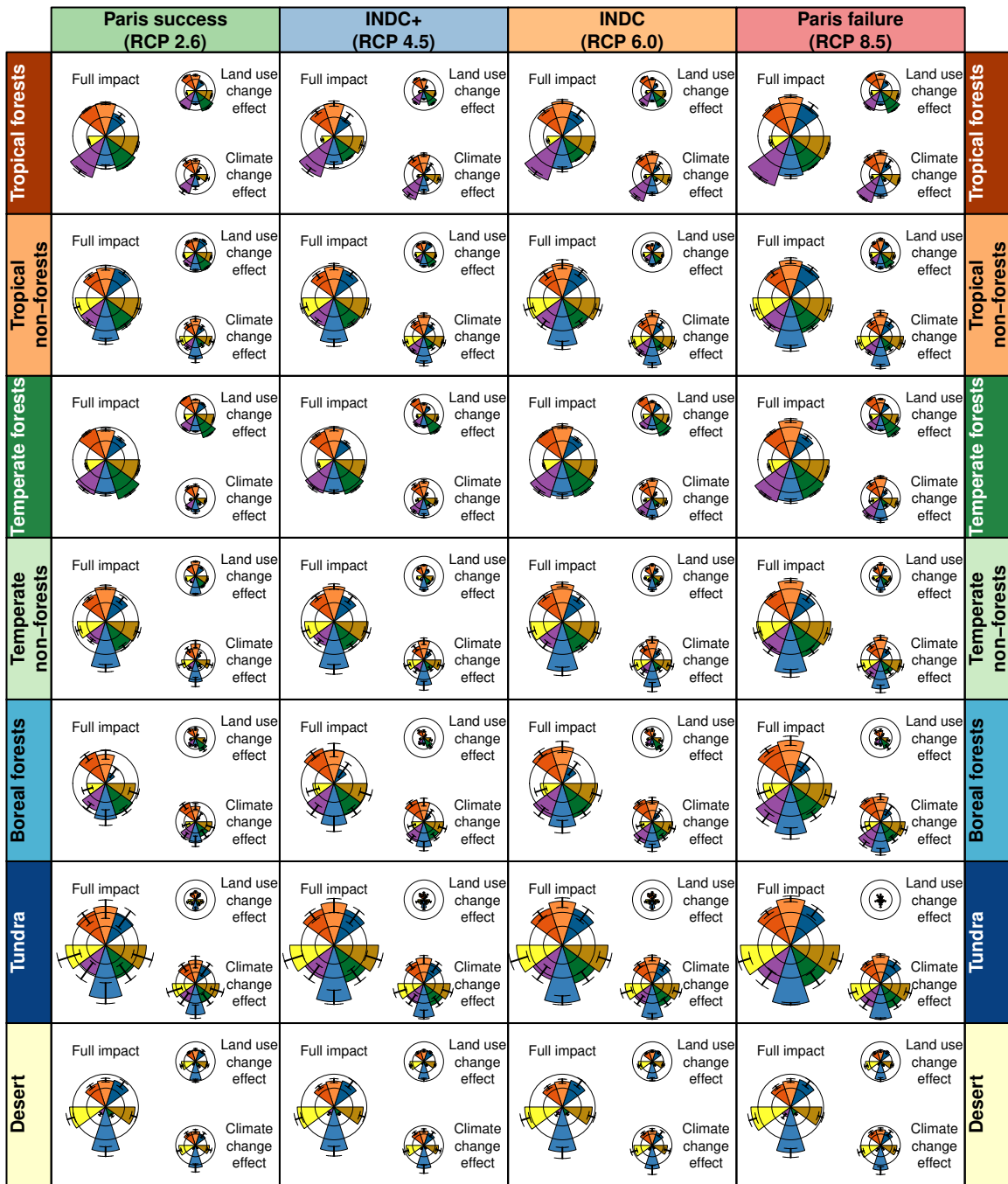
Figure S7. Decomposition of Γ values for major biomes. Components ecosystem balance $b \cdot S(b, \sigma_b)$, global importance $g \cdot S(g, \sigma_g)$, local change $c \cdot S(c, \sigma_c)$ and vegetation structure $\Delta V \cdot S(\Delta V, \sigma_{\Delta V})$ are combined into the full Γ metric. Values for carbon stocks, carbon fluxes and water fluxes illustrate the relative contribution of different processes to the full metric. Pies denote ensemble mean while whiskers show range across 20 climate models.
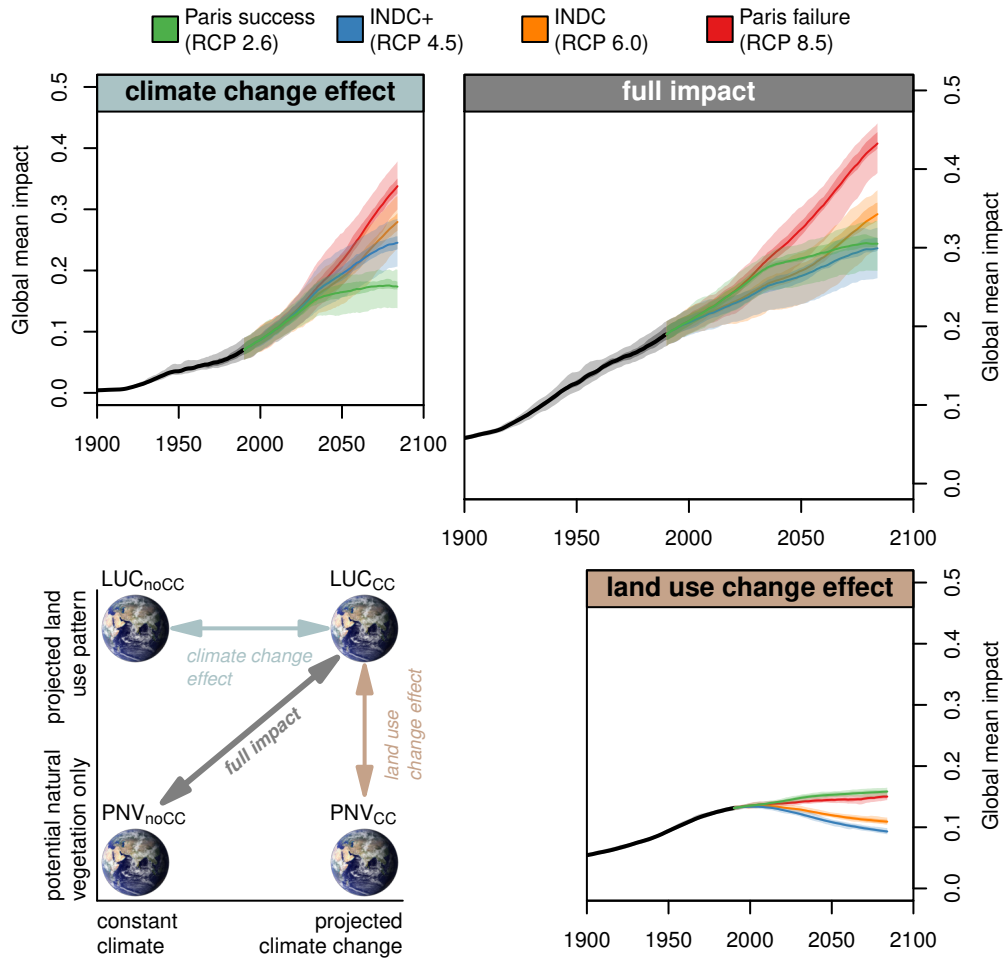
Figure S8. Global mean impact of climate change and land use change on the biosphere. Analogous to Figure 1 in the main text, climate change effect and land use change effect describe the individual impacts of CC and LUC while the full impact measures the combined effect of both drivers. Instead of using a threshold to distinguish areas with major impacts, Γ values in each landscape (grid cell) are averaged using an area-weighted mean. Earth image by NASA Goddard Space Flight Center.
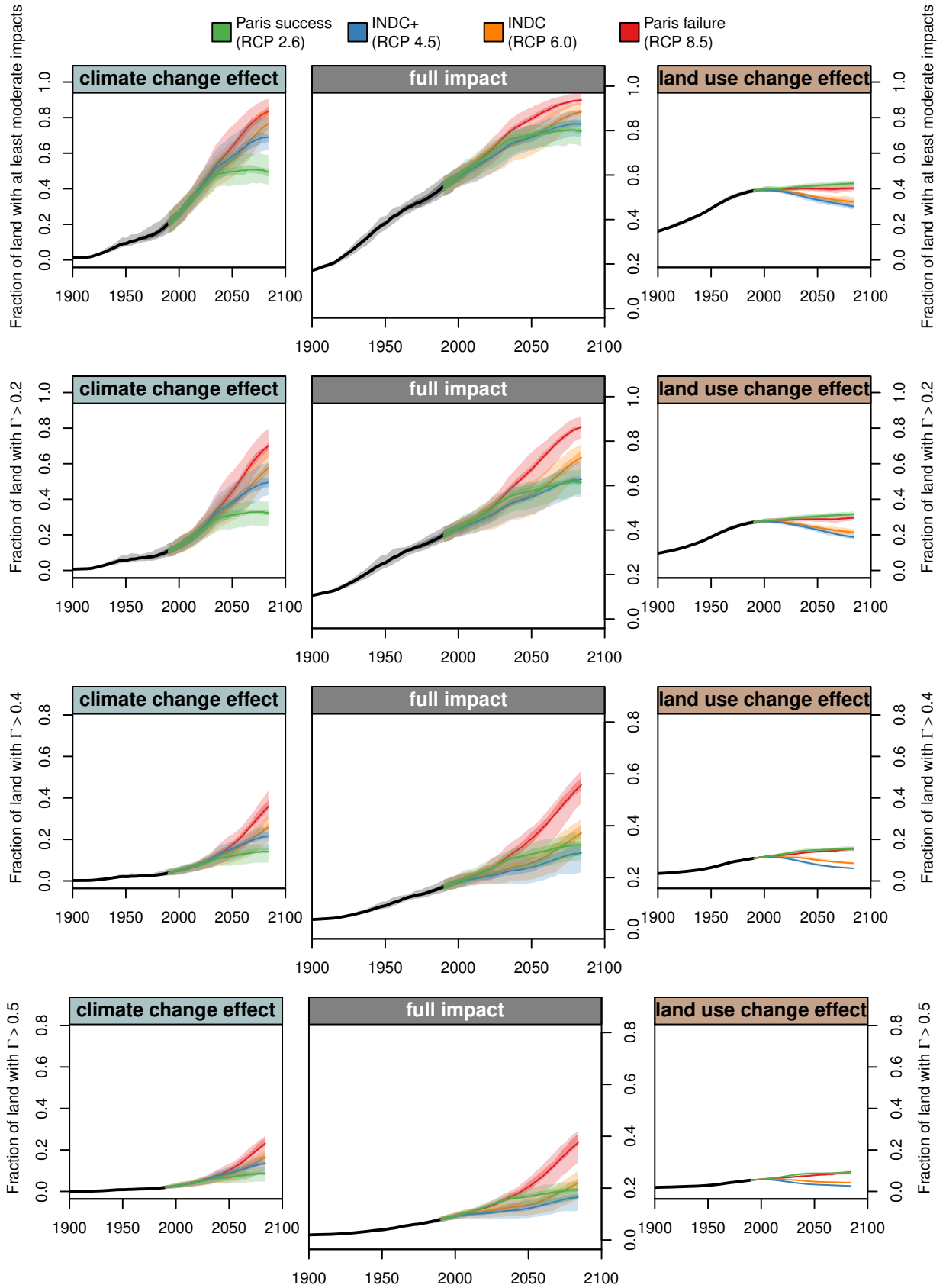
Figure S9. Sensitivity of the area with projected major impacts to the threshold used. Presentation as in Figure S8 and Figure 1 in the main text.

Table S1. Parameters describing landscape states in the Γ metric [modified after *Ostberg et al.*, 2015]. BFT, biomass-functional type; CFT, crop-functional type; PFT, plant-functional type.

Parameter group	Individual parameters
Carbon exchange fluxes	Net primary production, sum of heterotrophic respiration and harvest (from cropland, managed grassland and bioenergy plantations), fire carbon emissions
Carbon stocks	Carbon contained in vegetation, sum of litter and soils
Water exchange fluxes	Transpiration, sum of soil evaporation and interception loss from vegetation canopies, runoff
Other system-internal processes	Fire frequency, soil water content (upper 1 m)
Vegetation structure	Composition of BFTs, CFTs and PFTs

Table S2. Plant-functional types, *crop-functional types* and biomass-functional types and their assigned attributes [modified after *Ostberg et al.*, 2015]. PFT and BFT abbreviations: TrBE, tropical broadleaf evergreen tree; TrBR, tropical broadlead raingreen tree, TeNE, temperate needleleaf evergreen tree; TeBE, temperate broadleaf evergreen tree; TeBS, temperate broadleaf summergreen tree; BoNE, boreal needleleaf evergreen tree; BoS, boreal summergreen tree; TrBi, tropical bioenergy tree; TeBi, temperate bioenergy tree.

Lifeform	Attributes				
Tree:	**Evergreenness**	**Needleleavedness**	**Tropicalness**	**Borealness**	**Naturalness**
TrBE	1	0	1	0	1
TrBR	0	0	1	0	1
TeNE	1	1	0	0	1
TeBE	1	0	0	0	1
TeBS	0	0	0	0	1
BoNE	1	1	0	1	1
BoS	0	0.25*	0	1	1
TrBi	1	0	1	0	0
TeBi	0	0	0	0	0
(attribute weights:	0.2	0.2	0.3	0.3	0.3)

Grass:	**Tropicalness**	**Naturalness**
C3 grass	0	1
C4 grass	1	1
Temperate Cereals	0	0
Rice	1	0
Maize	1	0
Tropical Cereals	1	0
Pulses	0.5	0
Temperate Roots	0	0
Tropical Roots	1	0
Sunflower	0.5	0
Soybean	1	0
Groundnut	1	0
Rapeseed	0.5	0
Sugarcane	1	0
Others	0.5	0
Managed grass	**	0
Bioenergy grass	1	0
Grass under bioenergy trees***	**	0
(attribute weights:	0.3	0.3)

* BoS primarily represents broadleaved trees, but includes larchs.
** Derived from relative share of C4 grasses as determined dynamically by LPJmL.
*** Grass under bioenergy trees is not harvested.